3

A Few Afterglows With Hard Electron Energy Spectrum

3.1 Non-universality of p

Though numerical studies of particle acceleration in ultra-relativistic shocks produce values of p clustered around 2.2 (see Kirk & Duffy [77] for a review), several astrophysical sources display a broader distribution in their spectral index.

Active Galactic Nuclei (AGNs), Pulsar Wind Nebulae (PWNs) and GRBs, the common harbours of relativistic shock acceleration sites, do not favour a universal power law for the resultant electron distribution. For many of these sources, the distribution of p is found not to be a δ-function, but a broad one with a $\sigma_p \sim 0.5$ [122]. The value of p is not only spread between 2.0 – 3.0, the range which numerical simulations prefer, but also goes below 2.0, to produce hard electron spectra (see chapter 2). Plerions, a subclass of PWNs have been well known to exhibit hard electron energy spectra. The Galactic plerions display a flat radio spectrum with an index of 0. – 0.3, which requires a p of 1.0 – 1.6. The origin for such a flat electron spectrum is still not fully understood and additional acceleration mechanisms are conjectured (See Arons [4]).

3.2 Shallow evolution for GRB AGs

For GRB afterglows, it is not often very easy to infer the value of p unambiguously. The spectral index from the optical bands is a composite of the unknown host galaxy extinction and the intrinsic δ. The X-ray spectrum is not affected by dust extinction but is modified by photoelectric absorption at lower energies. This makes the x-ray spectral index to be a function of the unknown gas column density along the line of sight. Also, due to the low count rate, it is often difficult to bin the spectrum and get the value of δ accurately. A third method is to measure the flux decay index past the jet break in optical and in x-ray wavelengths and assume it to be p, as predicted by the standard afterglow model. Though it suffers from complexities in the modelling of the fireball dynamics, like smoothening of the jet break etc., this method is largely followed and trusted. However, the spectral index derived should be consistent with the α–δ relations in various bands.

Zeh et al. [145] have collected data for 59 pre-*Swift* afterglows based on well sampled optical and IR lightcurves. The afterglows show a wide range of post break index values, which if identified as p is an indication of such a range in the p-values too. In table 3.1, we list the afterglows from this collection, which shows shallow post-break decay slopes.

Shen et al. [122] along with blazars and PWNs, present a sample of well monitored X-ray afterglows. The inferred values of p fall below 2 for eight of them (See figure 5 of Shen et al. [122]).

Early evolution of several x-ray afterglows monitored by *Swift* have shown an unprecedented 'flat' evolution [93]. Though not all of them may have an intrinsic flat electron energy spectrum (some could be show shallow decay due to prolonged energy injection from the central engine), some are well within the expectations of flat spectrum models. From the sample of 27 *Swift* afterglows from Nousek et al. [93], we find at least 3 of them consistent with the α-δ relations for $p < 2$ derived in the previous chapter. We list these afterglows also in table 3.1

Out of the 19 afterglows listed in table 3.1, we select three of them (GRB010222, GRB020813 and GRB041006) based on the availability of rich multiband data necessary for reaching a conclusion about the underlying flat electron energy spec-

GRB name	α_1	α_2	t_j (day)	reference
980703	0.85 ± 0.84	1.65 ± 0.46	1.35 ± 0.94	[145]
990123	1.24 ± 0.06	1.62 ± 0.15	2.06 ± 0.83	[145]
991216	1.17 ± 0.03	1.57 ± 0.03	1.10 ± 0.13	[145]
010222	0.60 ± 0.09	1.44 ± 0.02	0.64 ± 0.09	[16, 145]
020124	1.47 ± 0.06	2.12 ± 0.27	1.36 ± 0.77	[145]
020331	0.69 ± 0.04	2.12 ± 0.40	7.17 ± 1.52	[145]
020405	1.26 ± 0.09	1.93 ± 0.13	2.40 ± 0.45	[145]
020813	0.67 ± 0.07	1.78 ± 0.28	0.77 ± 0.25	[145]
021211	0.96 ± 0.04	1.22 ± 0.10	0.11 ± 0.09	[145]
030328	0.87 ± 0.04	1.54 ± 0.11	0.60 ± 0.10	[145]
030418	1.23 ± 0.09	1.72 ± 0.48	1.50 ± 1.26	[145]
030725	0.80 ± 0.06	1.65 ± 0.06	2.9 ± 0.0	[145]
041006	0.68 ± 0.06	1.30 ± 0.02	0.23 ± 0.04	[91, 145]
050318	1.00 ± 0.1	1.77 ± 0.06	0.12 ± 0.001	[93]
050319	0.47 ± 0.1	1.2 ± 0.25	0.46 ± 0.003	[93]
050505	$0.66^{+0.13}_{-0.12}$	$1.72^{+0.11}_{-0.08}$	$0.23^{+0.06}_{-0.03}$	[93]
	value of p from model			
990510	$1.83^{+0.18}_{-0.01}$			[97]
991208	1.53 ± 0.03			[97]
000301c	$1.43^{+0.05}_{-0.07}$			[97]

Table 3.1. Afterglows which show shallow temporal decay. Those referred to Nousek et al. [93] are selected based on their x-ray evolution. GRBs referred to Panaitescu & Kumar [97] are based on the multiband modelling done by the authors. The rest are optically selected by Zeh et al. [145]

trum. In the following sections we present the model and best fit parameters of these afterglows.

3.3 GRB010222

The Gamma Ray Burst of 22nd February 2001 was detected by Gamma Ray Burst Monitor and Wide Field Camera on board the satellite BeppoSAX at UT February 22nd 07:23:30 [105]. The source location was identified as RA = $14^h52^m12.54^s$ and DEC = $+43°01'6.2''$(J2000) by further observations [67]. A bright X-ray afterglow was detected soon [66], which was followed up in optical, submm, NIR, and radio bands [10, 38]. Absorption lines with a redshift of 1.477 against the optical transient was detected [75, 90] which placed the burst at a luminosity distance of 11.53 Gpc for assumed cosmological parameters $\Omega_\lambda = 0.7$, $\Omega_m = 0.3$ and $H_0 = 65$. Using the measured fluence of $(9.3 \pm 0.3) \times 10^{-5}$ erg cm^{-2}, the isotropic equivalent energy obtained for this burst equals $(3.97 \pm 0.3) \times 10^{53}$ erg. The submm flux was persistent and is believed to be from the starburst host *SMMJ14522+4301* [46].

3.3.1 Multiband Modelling

GRB 010222 was one of the first afterglows seen with hard electron spectrum and it initiated theoretical work in that direction [15, 35]. The optical afterglow decay was shallow with $\alpha_1 \sim 0.6$ [116], which steepened to an α_2 of 1.3 - 1.4 after an early break around half a day. Sagar et al. [116] finds the spectral index within the optical band to be ~ 0.6. X-ray observations from BeppoSAX NFI shows a decay index ~ 1.3 which matches fairly well with the post break optical decay index [74]. Using the late observations of the SAX WFC, in't Zand et al. [74] obtains significant constraints for a break in the x-ray lightcurve. The prescribed break in x-rays happens around 0.5 days and the pre-break index is ~ 0.6, hence its achromatic nature is confirmed by the x-ray data.

Mirabal et al. [90] derives a Galactic extinction corrected spectral slope of -0.89 ± 0.03 for the whole duration of the burst, which is also in agreement with the δ derived by other optical studies [75, 126]. No signature of optical spectral

evolution is seen from any of these data sets.

The BeppoSAX x-ray spectrum (0.1 – 10 keV) is fitted with an absorbed power-law of slope $\delta \sim 0.97$ and a redshift corrected hydrogen column density $N_H \sim 2.5 \times 10^{22}$ cm^{-2} [74]. According to the authors the extrapolated optical spectrum falls much below the x-ray flux.

The achromatic nature of the lightcurve break suggests a jet geometry for the outflow and a hard electron distribution with index $p \sim 1.4$ for the radiating electrons. This requires dust extinction in the host frame which would have steepened the optical spectrum to have made its extrapolation fall below the simultaneous x-ray flux. In our model, a p of ~ 1.4, explains both x-ray and optical decay indices as both the bands lie above ν_c. The correction for the intrinsic extinction in the host flattens the optical spectrum to a δ of 0.7, which equals $p/2$, as expected for bands above the cooling frequency. The x-ray spectral index, δ_x is close to unity and is steeper than δ_o and also the δ (0.7) derived from p of 1.4. This motivates us to assume that the injection break lies in the x-ray band, steepening the spectral slope. We calculated the inverse compton emission for this model, following the method described in section 2.10 and found that it is negligible at the x-ray frequencies. The parameter set generated by the best fit model with a $\chi^2_{\rm dof}$ of 4.1 is given in table 3.2.

The optical flux of the host can be deduced from the late HST observations [52]. The radio flux is a mix of the starburst host and the afterglow. Frail et al. [46] present a host model combining synchrotron and black body spectrum for cm and submm bands. According to their model $F_{1.4\rm GHz}$(host) is 85^{+115}_{-50} μJy and the spectral index is -0.75. We considered host galaxy flux in BVRI bands as well as in radio (8.46 GHz and 4.86 GHz) as fit parameters. The $\sim 20\,\mu$Jy centimeter flux of the source, predicted by our best fit model is in good agreement with the values estimated by Frail et al. [46] and the predicted optical flux in BVRI bands agree well with those observed [52]. The fitted value of the host emission in these bands are given in table 3.2.

Another important point to note for this burst is the gas-to-dust ratio derived from the x-ray and optical spectra. The hydrogen column along the line of sight has a column density of $\sim 10^{22}$ cm^{-2} [74]. While the Galactic N_{HI} along this line

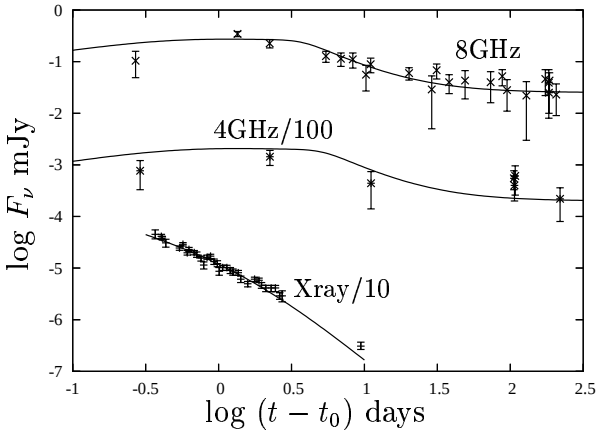

(a) Radio and x-ray lightcurves. The 4 GHz lightcurve and the 10^{18} Hz x-ray lightcurve are offset by 0.01 and 0.1 mJy respectively for the ease of viewing.

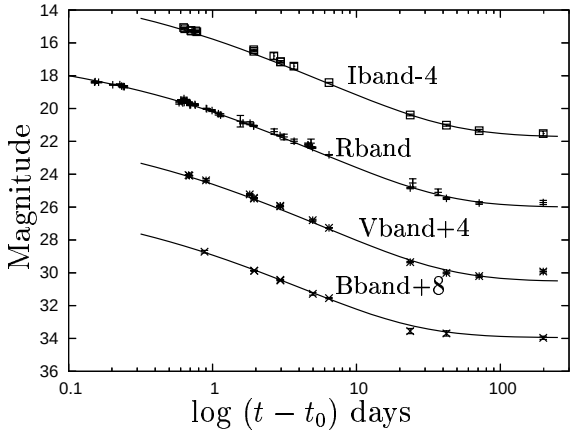

(b) Optical BVRI lightcurves, appropriately offset to avoid clustering.

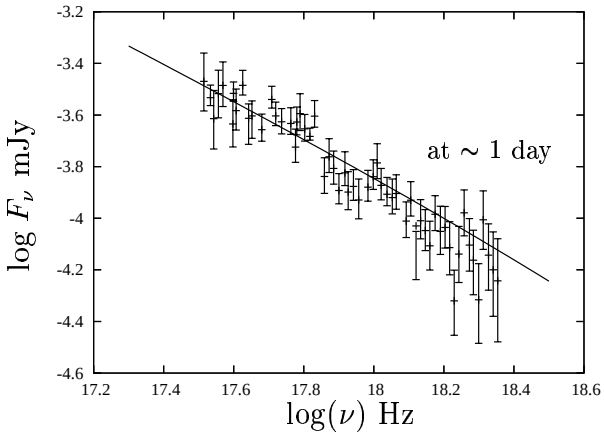

(c) X-ray spectrum at $\sim$ 1 day from BeppoSAX along with the model

Figure 3.1. Multiband model fits for GRB010222. Points : observed data. Solid line : our model. The flattening seen in radio lightcurves (panel a) are due to the flux of the starburst host SMMJ14522+4301 (see text for details).

of sight is roughly 10^{20} cm^{-2}, the additional gas column must be related to the host galaxy. We derive an E_{B-V} (host) of 0.01 and a starburst type extinction law for the dust distribution [26]. The above value of E_{B-V} is two orders of

magnitude low for the derived N_{HI} values if one assumes the normal dust to gas ratio seen in Milky Way type galaxies. ($N_{HI} = 5.3 \times 10^{21}$ cm^{-2} E_{B-V} [110]) This suggests that the nature of dust could be different in some GRB hosts.

Electron Distribution Parameters		Spectral Parameters (At ~ 0.7 days)	
p_1	$1.42^{+0.01}_{-0.02}$	ν_m	$1.77^{+9.4}_{-0.65} \times 10^{11}$ Hz
p_2	2.1 ± 0.05	ν_c	$7.1^{+1.8}_{0.78} \times 10^{13}$ Hz
q	1.0	ν_i	$9.26^{+2.41}_{-1.85} \times 10^{18}$ Hz
		f_m	$0.74^{+0.04}_{-0.27}$ mJy
Others			
t_j	0.70 ± 0.15 day	$E_{(B-V)}$ (host)	$0.01^{+0.02}_{-0.01}$ mag
Host Galaxy Flux			
B band	$25.64^{+0.5}_{-0.25}$ mag	V band	$26.29^{+0.25}_{-0.5}$ mag
R band	$25.83^{+0.25}_{-0.3}$ mag	I band	25.59 ± 0.25 mag
8.46 GHz	$25^{+25}_{-19}\mu$Jy		
4.86 GHz	$20^{+59}_{-10}\mu$Jy		

Table 3.2. The fit parameters for GRB010222, given at the time of the jet break.

n(assumed)	1.0 atom/cc
ϵ_e	~ 1.0
ϵ_B	$0.03^{+0.007}_{-0.006}$
ξ	$9.5^{+1.3}_{-1.5} \times 10^4$
$E_{\rm iso}$	$2.2^{+0.46}_{-1.8} \times 10^{52}$ ergs
θ_0	$2.3^{\circ +0.003}_{-0.004}$
$E_{\rm tot}$	$3.2^{+0.63}_{-1.6} \times 10^{49}$ ergs

Table 3.3. The physical parameters for the afterglow calculated using the fit parameters shown in Table 3.2. Since ν_a was not constrained, we assumed n to be 1.0 atom/cc and calculated the rest of the parameters.

3.3.2 Discussion

In the previous section, we have presented the modelling of this afterglow based on hard electron energy spectrum. However, there have been other attempts to

model it using a standard steep electron energy spectrum.

Masetti et al. 2001 [88] assumed the outflow to be spherical and considered the achromatic break to be due to the non-relativistic transition of the fireball. The assumptions yielded a p of 2.1 - 2.2 from the observed α_1 and α_2. With considerable extinction in the host($E_{(B-V)} \sim 0.35$) this would satisfy the observed steep ($\delta \sim 1.2$) optical spectrum. But for the burst energy of 7.7×10^{53} derived from the fluence using a luminosity distance d_L of 11.53 Gpc, the ambient medium density required to slow down the relativistic fireball into newtonian phase by ~ 1 day is very high. Adopting the expression $t_{NR} = 12(1+z)(E_{52}/n)^{1/3}$ day , one obtains $n \sim 10^6$ atom/cc (Masetti et al. quotes an n of $10^5 - 10^6$ atom/cc for a non-relativistic transition of $\sim$ 1 day [88]). However, such a high ambient medium density produces an optically thick fireball even at high frequencies and the model would not have been able to reproduce the radio observations reported later. The synchrotron self absorption frequency derived for the above values of E_{52} and n is $\sim 10^{11}$ Hz at ~ 1 day, and the expected flux at 8.4 GHz will be of nano-jansky level, against the observed value of 0.1 – 0.3 mJy flux.

Björnsson et al. [17] modelled the observations assuming continuous injection of energy from the central engine to be the cause of the shallow decay. Their analysis of the Chandra X-ray spectrum yielded an index of ~ 0.7 (the BeppoSAX δ_x is ~ 1.0) with redshift corrected N_H column density of 6.5×10^{21} cm^{-2} in the host (in't Zand et al. [74] obtains a N_H of $\sim 2.5 \times 10^{22}$ cm^{-2}). They mention that if N_H is fixed at the valued used by [74], the δ obtained will be consistent with the BepoSAX results. With $\delta \sim 0.7$ and considerable optical extinction in the host frame due to dust, and assuming both optical and x-ray bands below ν_c Björnsson et al. [17] fit the data with a continuous energy injection model with a steep electron energy spectrum ($p \sim 2.5$). We find, even if the x-ray spectral index is flatter, it is still within the predictions of the model we presented, with the injection break moved to energies higher than x-ray. The simplest interpretation of the evolution of this afterglow involves an intrinsically hard electron energy spectrum.

Model fitting to multiband observations of most GRB afterglows produce the fireball kinetic energy, $E_{\rm kin}$ similar to the energy released in radiation, in the

prompt phase, $E_{\rm rad}$, although theories do not necessarily predict this. In the present case, we derive an $E_{\rm iso}$ of $\sim 10^{52}$ ergs which is an order of magnitude less the than the isotropic equivalent energy in radiation, which is an interesting feature to notice.

The best fit model along with the observations are displayed in figure 3.1. The spectral parameters and physical parameters are listed in table 3.2, and table 3.3 respectively.

3.4 GRB 020813

This GRB was detected by *HETE-II* on 2002 August 8th at 2:44 UT [139]. It was a bright long duration event with a 30–400 keV fluence of $(2.53 \pm 0.07) \times 10^{-5}$ ergcm^{-2} and $T_{90} = 125$ s [73]. The optical candidate was soon identified at RA $= 19^h46^m41.9^s$ and Dec$= -19^\circ36'4.8"$ [44]. The burst redshift was inferred to be $z = 1.26$ by spectroscopic observations at the KECK telescope (Barth et al.). This will correspond to a luminosity distance of 9.43 Gpc for H_0 of 65., $\Omega_\lambda = 0.7$ and $\Omega_m = 0.3$. The isotropic equivalent energy is deduced to be $(1.2 \pm 0.07) \times 10^{53}$ ergs. The afterglow was also detected by Chandra [137] and the VLA [45]. Only upper limits were available in the millimeter band [14, 22]. The optical afterglow of this burst is examined for fluctuations in magnitude by high precision photometry and is found to be smooth upto 0.5% during the span of observation [82], as opposed to some other afterglows identified with variabilities of the order of 10% or more (for example, GRB021004 [100]). However, several absorption line systems resembling that of GRB021004 are identified against the optical afterglow, by VLT [42] and Keck [120] telescopes. The optical polarisation lightcurve for this afterglow is also available, though sampled sparsely [8, 58].

3.4.1 Multiband Modelling

The optical afterglow of GRB020813 also exhibited similar shallow decay index and an early break like that of GRB010222 ($\alpha_1 \sim 0.8$, $t_b \sim 0.5$ day in optical [31]). The x-ray observations started after the break detected in optical and the lightcurve followed a single power law decay consistent with the post break

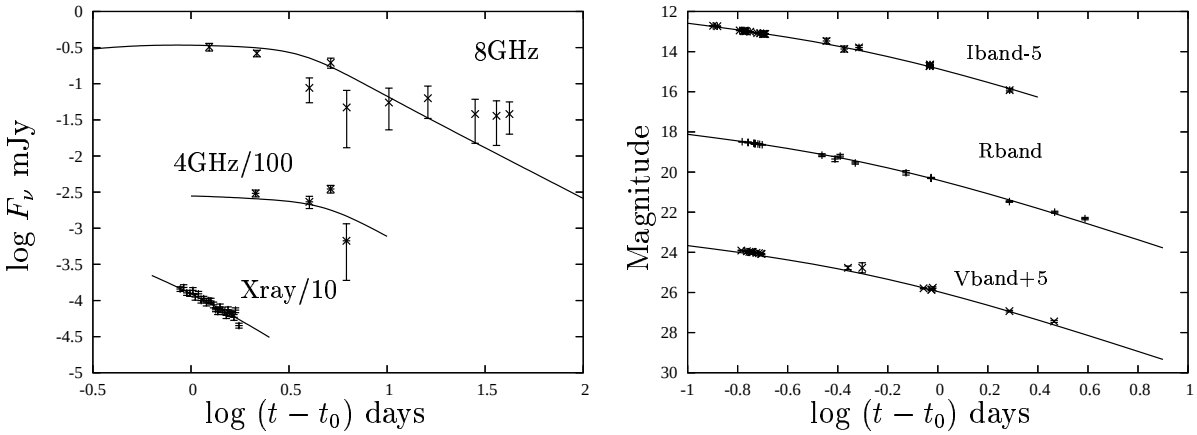

Figure 3.2. GRB020813: Best fit model along with the observations. (i)The top two curves in the left side panel are radio flux in 8.46 GHz and 4.86 GHz respectively. For ease of viewing, 4.86 GHz flux is shown with an offset of 0.01 mJy. The late time flattening in the 8 GHz data is not due to the presence of any host. Such flattening is seen in the radio afterglows beyond a few days past the burst, and is suspected to be some non-standard behaviour (see Frail et al. 2004) which is not taken care of by our code. The bottom curve in this panel is the x-ray lightcurve at 1.2×10^{18} Hz. (ii) The right side panel displays the optical multiband lightcurves. I band is offset by -5 magnitudes while V band is off set by $+5$ magnitudes

optical decay ($\alpha_o \sim 1.4$ [31], $\alpha_x \sim 1.4$ [24]). The optical photometric spectral index, corrected for Galactic absorption was ~ 0.9 [31] and the x-ray spectral index was ~ 1.0 [24] with no absorption column in excess of the Galactic value of 7.5×10^{20} cm^{-2}.

The value of p obtained from the best fit model is 1.4, for a $q = 1$. The jet break is around half a day. We assumed ν_c to be $\sim 3 \times 10^{13}$ Hz at the time of jet break, below the optical bands, to satisfy the observed α and δ in both x-ray and optical. Synchrotron peak frequency ν_m is around 3×10^{11} Hz at the time of the jet break and the peak flux f_{ν_m} is ~ 1 mJy. There is no signature of the injection frequency, unlike GRB010222, within available observations. The self absorption frequency ν_a cannot be constrained using current observations. Our model requires additional extinction from the host, with rest frame A_v of 0.09 corresponding to an E_{B-V} of 0.04 and a starburst type extinction law [26]. Savaglio & Fall [120] presenting the KECK spectroscopy of this afterglow, argues for a heavy extinction of the afterglow in the host galaxy due to its dust content.

Electron Distribution Parameters		Spectral Parameters (At ~ 0.5 days)	
p_1	$1.40^{+0.02}_{-0.005}$	ν_m	$3.06^{+6.73}_{-0.64} \times 10^{11}$ Hz
p_2	~ 2.1	ν_c	$3.53^{+0.92}_{-1.31} \times 10^{13}$ Hz
q	1.0	ν_i	$> 2.5 \times 10^{19}$ Hz
		f_m	$1.07^{+0.11}_{-0.57}$ mJy
Others			
t_j	$0.53^{+0.05}_{-0.03}$ day	$E_{(B-V)}$ (host)	0.04 ± 0.01 mag

Table 3.4. Model Parameters of GRB020813, at the time of the jet break. No signature of the injection break is seen during the span of the observations, hence we obtain only a lower limit for it, which in turn has provided a lower limit for ξ (see next table)

n(assumed)	0.1 atom/cc
ϵ_e	~ 1.0
ϵ_B	$0.08^{+0.01}_{-0.03}$
ξ	$> 1.1 \times 10^5$
$E_{\rm iso}$	$2.97^{+0.5}_{-1.9} \times 10^{52}$ ergs
θ_0	$2.2^{\circ}{}^{+0.001}_{1.35}$
$E_{\rm tot}$	$2.2^{+0.4}_{-1.5} \times 10^{49}$ ergs

Table 3.5. The physical parameters calculated from the fit parameters. As in the previous case, we assumed the value of ambient medium density

The value of A_v they obtain from the analysis based on column densities of several metal lines, is 0.4. This results from assuming a Milky Way type gas-to-dust ratio for the host, which is probably inappropriate for GRB hosts. Most GRB hosts instead display a very low gas-to-dust ratio (also see the other two GRBs discussed in this chapter) and reddening of 0.4 mag need not be present. In fact, Savaglio & Fall [120] themselves derive a very low host extinction as well as absence of the 2715 A° from the UV continuum fittings, which support this inference.

3.4.2 Discussion

GRB020813 is yet another example of hard electron energy spectrum afterglows. Not many attempts have so far been made in its multiband modelling. We have

presented here our attempt at modelling of the afterglow using an electron energy distribution function with index ~ 1.4. In this model, we find that the cooling frequency falls below the optical band within 2 hours since burst. The inferred isotropic equivalent energy (kinetic) is an order of magnitude less than that of radiation as in GRB010222. The polarisation lightcurve of this afterglow has been explained in terms of a structured jet [83]. The lightcurve from a structured jet viewed at an angle θ_0 hardly differs from that of a homogeneous jet with half opening angle θ_0 [113] (especially for a jet structure described by a θ^{-2} powerlaw). Hence we can still safely assume the shallow powerlaw model for the electron energy distribution within the jet, eventhough we are not using the structured jet calculations. However, The total energy calculations will be affected, if the energy distribution is not homogeneous within the jet. If we assume that our inferred value of θ_0, is approximately equal to the half opening angle of the core of the structured-jet [113], and if the actual extent of the jet is 90°, the energy inferred will be ~ 9 times smaller than the true energy (see Rossi et al. for details).

The best fit model along with the observations are displayed in figure 3.2. The spectral parameters and physical parameters are listed in table 3.4 and table 3.5 respectively.

3.5 GRB041006

GRB 041006 was detected by the High Energy Transient Explorer (HETE II) Fregate and WXM instruments at 12:18:08 UT on 06 October 2004 [54]. Its fluence in 2−30 keV and 30−400 keV bands were 5×10^{-6} erg/cm^2 and 7×10^{-6} erg/cm^2 respectively which classifies this as an "x-ray rich GRB". A fading x-ray counterpart was reported [23] and the optical afterglow located at $\alpha = 00^{\rm h}54^{\rm m}50^{\rm s}.17$, $\delta = +01°14'07"$ (J2000) was found [34]. Using the redshift of $z = 0.712$ [51], and the fluence reported by [54], we calculate an isotropic equivalent gamma ray energy of 2.9×10^{52} ergs for this burst.

3.5.1 Multiband Modelling

The optical afterglow of GRB041006 exhibited a relatively flat decay $\alpha_1 \sim 0.5$ in the early phase which steepened to $\alpha_2 \sim 1.3$ after a break around 0.14 day [125, 128]. If this is the jet break, the indices indicate a hard electron energy spectrum for the synchrotron emitting electrons. At 0.058 day the intrinsic spectral index of the afterglow was 0.685 ± 0.13 between B and V bands [33]. At 1.74 day, the index became 1.0 ± 0.18 between B and R bands (Garnavich et al. 2004). But this is only a marginal steepening, seen within one sigma error. The x-ray spectral index of 0.9 ± 0.2 measured at 1.23 days [33] is consistent with the δ observed within the optical bands. Hence, the reported spectral indices in both optical and x-ray bands support the inference of a hard electron energy spectrum with index ~ 1.3, if both the bands are above ν_c. The x-ray lightcurve follows a single power law of slope -1.0 ± 0.1 during 0.7 to 1.7 days [25]. This indicates that the x-ray flux decay is slower than the optical. But using the same data presented by Butler et al. we find that a powerlaw of slope close to 1.4 could also describe the flux evolution fairly well. Apart from the optical and x-ray observations, upper limits to the afterglow flux are available in NIR [76], millimeter [6, 7] and radio [124] wavelengths.

We assume the cooling frequency (ν_c) to be below the optical bands to satisfy α of 0.5 and δ in the range of $0.6 - 0.7$ simultaneously. Similar to GRB020813, there is no signature of steepening seen at the higher energy end of the spectrum from the available observations. Hence we place ν_i above x-ray band. We compute the spectral evolution of the afterglow with these basic assumptions.

After excluding the NIR/mm/radio upper-limits and the optical data beyond 5 days (where a supernova bump prominently appears) from the fit, the model converged to a minimum $\chi^2_{\rm DOF}$ of 3.4. An additional extinction other than that due to Galactic dust (A_V of 0.07 mag, estimated for this direction [121]) is required by the model, which could result from the dust distribution in the host galaxy of the GRB. We obtained A_V in the range of $0.03 - 0.16$ mag in the host rest frame, assuming a Galaxy type extinction law for the dust distribution [27]. According to Butler et al. [25] the x-ray spectrum is well fit by an absorbed power-law with the neutral hydrogen column density (N_H) greater than that expected

from the Galactic column along the line of sight. They estimate an excess N_H of 3.2×10^{21} cm^{-2} for the host rest frame. The rest frame $E_{(B-V)}$ to N_H ratio is two to three orders of magnitude smaller than the empirical value obtained for the ISM of our galaxy [110]

Electron Distribution Parameters		Spectral Parameters (At 0.1 days)	
p_1	$1.29 - 1.32$	ν_m	$(1.2 - 3.0) \times 10^{12}$ Hz
p_2	> 2.2	ν_c	$(1.0 - 2.0) \times 10^{14}$ Hz
q	1.0	ν_i	$> 2.4 \times 10^{20}$ Hz
t_j	$0.17 - 0.24$ day	f_m	$(0.37 - 0.49)$ mJy
Others			
$E_{(B-V)}$ (host)	$0.01 - 0.05$ mag		

Table 3.6. The fit parameters around the time of jet break. Here also, like GRB020813, we do not see the injection break passing. A lower limit of $\sim 10^{20}$ Hz is placed based on the x-ray observations

n(assumed)	1.0 atom/cc
ϵ_e	~ 0.8
ϵ_B	$0.07 - 0.14$
ξ	$> 2.0 \times 10^4$
$E_{\rm iso}$	$(2.0 - 4.0) \times 10^{51}$ ergs
θ_0	$1.7^\circ - 2.8^\circ$
$E_{\rm tot}$	$(1.4 - 3.4) \times 10^{48}$ ergs

Table 3.7. The physical parameters obtained for the burst. Like the previous GRBs, here too value of n is assumed

Since available observations do not cover the 0.12 day break in various bands, its achromatic nature as expected for a jet break, cannot be confirmed. As a mild evolution in the optical spectral index between 0.06 days to 1.7 days has also been reported, we examined the possibility of the temporal steepening arising from the passage of a spectral break through R-band. The observed change in α is ~ 0.8 and the maximum change that could be attributed to δ is 0.3. Passage of the cooling frequency would predict $\Delta\alpha = 0.25$ and $\Delta\delta = 0.5$, and hence can

not reproduce the observed α and δ. The only other possibility is the passage of the injection break through R-band around 0.1 day, with p_1 being ~ 1.3 and $p_2 \sim 2.3$. A model with this assumption can reproduce the optical observations and the NIR/mm/radio upper limits very well but it underpredicts the x-ray observations by two orders of magnitude, requiring a substantial contribution from inverse-compton emission. The inverse compton contribution calculated using our model parameters are insignificant in the observable bands.

We find from our analysis that the best possible explanation for the multi wavelength observations for this afterglow is the synchrotron emission from a collimated outflow with electrons distributed in a hard energy spectrum.

3.5.2 The Associated Supernova

The afterglow optical flux decay showed deviation from a powerlaw behaviour after ~ 0.5 days and exhibited a bump around 25 days. Stanek et al. [128] attributes this behaviour to the emission from an associated supernova. We subtracted the modelled power-law flux and an assumed host galaxy flux (for which no direct measurement is available) from the observed emission to estimate the supernova contribution. Stanek et al. [128] find that the supernova associated with GRB 041006 peaks at a later (1.35 times) time after explosion and is also brighter in comparison to SN1998bw redshifted to $z = 0.716$. The late HST observations (mainly I band) show that the supernova is ~ 0.3 magnitudes brighter than a k-corrected SN1998bw whilst no additional stretch in time is required [125]. The authors also point out the possibility of the late time flux being contaminated by the host and also by a nearby galaxy.

The major difference our afterglow model has, in this context, is the presence of the host extinction (rest frame $A_V = 0.1$ mag in the best fit model). We used the late time observed magnitudes in R-band [128] and in I band [125] and subtracted the afterglow model flux to obtain the residual flux, which could be attributed to the associated supernova after subtracting the host galaxy flux. We used a SN1998bw lightcurve template with four free parameters (host galaxy flux in both the bands, Δm, the shift in magnitude required and $\delta - t$, a multiplication factor for the time axis) and performed a linear least square fit. The template

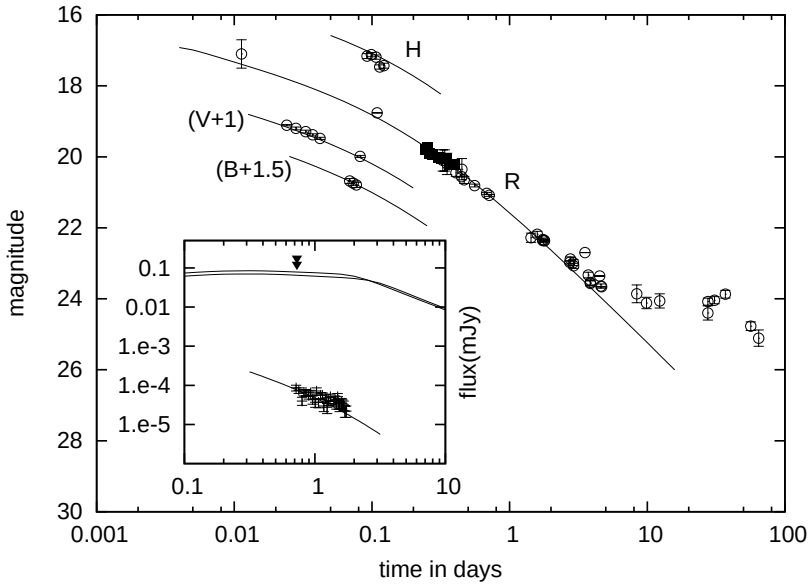

Figure 3.3. GRB 041006 afterglow observations in different bands along with the model. Light curve in different bands are shifted as indicated. Inset : X-ray observations and radio upper limits along with the model.

matches best with the associated SN lightcurve for Δm in the range (one sigma) of -0.55 to -0.75, $\delta - t$ between 1.05 and 1.1, R(host) in the range of 26.2 to 28.8 mag and I(host) between 26.8 and 28.9 mag (figure 3.4). From the figure, it appears that the I band data fits better with the template compared to the R band. We notice that a different value of Δm and $\delta - t$ would be required to fit the R band better, which suggests that the associated SN may have a different spectrum compared to that of SN1998bw. This could also be the reason for the different conclusions about the peak time and brightness of the associated supernova as mentioned above [125, 128].

3.5.3 Discussion

The decay index of ~ 1.3 seen in GRB 041006 afterglow lightcurve, post the one day break, suggests that the underlying electron energy spectrum could be hard ($p \sim 1.3$). A different model attributes this behaviour to the jet being viewed off-axis [60]. In this model, the ~ 0.1 day break is caused by the lorentz factor falling

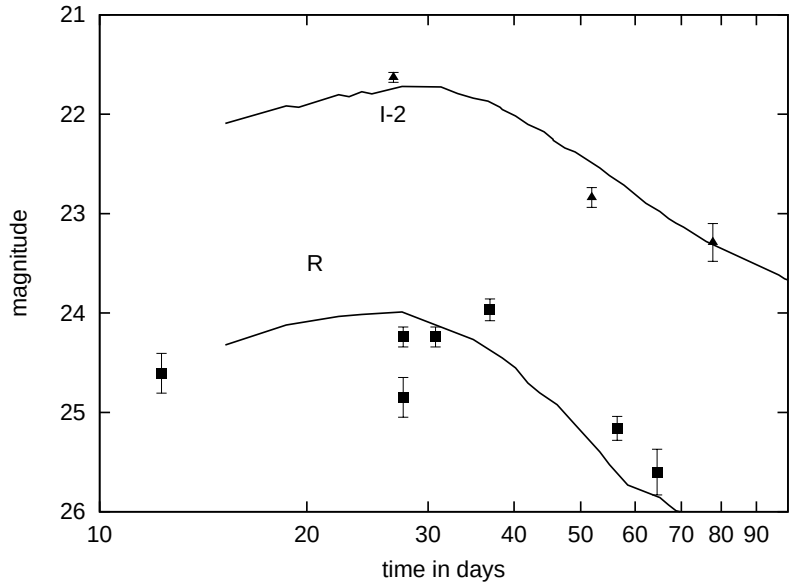

Figure 3.4. Comparison between the associated supernova in R (squares) and I (triangles) bands with the redshifted k-corrected SN1998bw (line) after applying a Δm and $\delta - t$ correction (see text). The curves have been shifted as indicated.

below the inverse of the viewing angle, there is no lateral expansion of the jet observed and the derived electron energy distribution is steeper ($p \sim 2.2$). They invoke the presence of a stellar wind driven ambient density profile to explain the reported x-ray decay index ($\alpha_x \sim 1.1$) which is smaller in comparison to the simultaneous optical decay index ($\alpha_o \sim 1.3$).

Since we do not find the x-ray decay to be flatter than the optical decay (see section on modelling), we used a normal ISM density profile for the ambient medium. The kinetic energy derived for the explosion is rather small (10^{48} ergs). With the available set of data, it is impossible to discriminate between the two models. However, both off-axis jets and wind driven density profiles, although realistic, are not inferred commonly from the afterglow models. For this afterglow, in fact, there is no need of going beyond the simplistic assumption of an on-axis jet ploughing through a constant density interstellar medium, if one assumes a flatter electron energy spectrum with an appropriate upper cut off at higher energies.

Butler et al. [25] extrapolate the observed optical spectrum, which has an index δ_o of -1.0 ± 0.1 to the x-ray frequencies and find that the observed x-ray flux is underpredicted. They suggest that a possible explanation for this and also for the smaller α_x could be the presence of considerable amount of inverse compton emission in the x-ray bands. They also find that the spectral index within the x-ray band ($\delta_x \sim 0.7$) is smaller than that within the optical band ($\delta_o \approx -1.1 \pm 0.1$). In our model, we have a hard electron energy spectrum, δ is close to 0.7, and the presence of extinction in optical bands due to dust in the host galaxy, explains the observed higher optical δ. After extinction correction, our model does not underpredict the observe x-ray flux, even though the inverse compton emission predicted by the model is negligible at the x-ray frequencies.

The best fit model along with the observations are displayed in figure 3.3. The spectral parameters and physical parameters are listed in table 3.6 and table 3.7 respectively.

3.6 Conclusion

In this chapter we have modelled three afterglows which showed strong evidence for hard electron energy spectrum. We assumed the value of q to be unity. For one of the afterglows (GRB010222), we have attempted a fit with a q of 0.5, but found that $q = 1$ gives a better fit. The passage of the 'injection break' through x-rays is seen for GRB010222, and that allowed us to estimate ξ.

For none of the three afterglows, the synchrotron self absorption was well constrained. This left us with four observables and five unknowns, and we assumed the value of ambient density n to obtain the rest of the physical parameters.

Though all of these afterglows were bright in their γ-ray output with isotropic equivalent energy in γ-rays to be 10^{52} – 10^{53} ergs, the total kinetic energy derived from multiband modelling is relatively low (10^{48} – 10^{49} ergs). This is partly due to the narrow beaming angle derived from an early jet break (for all the jets, θ_0 is roughly 2.5°). Perhaps kinetic energy being an order of magnitude less than the energy output in radiation, could be a trait associated with the presence of hard electron energy spectrum. More afterglows and their detailed modelling is

required to examine this possibility.

Another significant characteristic of all the three afterglows is a relatively low value of the synchrotron cooling frequency. While for most of the afterglows modelled in the literature, ν_c remain above optical bands even 1 day past the burst, all the afterglows discussed here have in our model, ν_c below the optical band within 3 hours past the burst.

For GRB010222 and GRB041006 we find a low gas-to-dust ratio from the model fittings. This might imply a different type of dust in the GRB host, and is not surprising if GRBs are to occur it star forming regions, where dust depletion is highly probable.

Appendix : Deriving Physical Parameters

For none of the three afterglows modelled in this chapter, the synchrotron self absorption frequency, ν_a was well constrained. Hence we assumed the value of n to obtain the remaining four physical parameters. The expressions used in deriving these physical parameters are given below. As described in the main text, the value of q has been assumed to be unity in deriving these expressions.

$$\mathcal{E}_{\rm iso,52} = n^{-0.2} \left[\frac{f_{\nu_m}}{C_f}\right]^{1.2} \left[\frac{\nu_c}{C_c}\right]^{0.4} \tag{3.1}$$

$$\epsilon_B = n^{-0.6} \left[\frac{f_{\nu_m}}{C_f}\right]^{-0.4} \left[\frac{\nu_c}{C_c}\right]^{-0.8} \tag{3.2}$$

$$\xi = n^{0.2} \left[\frac{f_{\nu_m}}{C_f}\right]^{-0.2} \left[\frac{\nu_c}{C_c}\right]^{0.1} \left[\frac{\nu_i}{C_i}\right]^{0.5} \tag{3.3}$$

$$\epsilon_e = n^{0.2} \left[\frac{f_m}{C_f}\right]^{-0.2} \left[\frac{\nu_c}{C_c}\right]^{0.1} \left[\frac{\nu_i}{C_i}\right]^{(2-p_1)/2} \left[\frac{\nu_m}{C_m}\right]^{(p_1-1)/2} \tag{3.4}$$

where, the coefficients C_m, C_c, C_f and C_i are the combination of numerical and physical constants in the expressions of the spectral parameters as given in section 2.8.3. However, for these expressions, since we adopted the equations for Γ, r and B from Wijers & Galama [142], these coefficients get slightly modified. They are given below.

$$C_m = 4.24 \times 10^9 \; x_{p_1} \; (1.+z)^{-1/2} \; \frac{m_p}{m_e} f_p^{\frac{2}{1-p_1}} \; t_d^{-1.5}$$

$$C_c = 1.12 \times 10^{12} \; \sqrt{1+z} \; t_d^{-0.5}$$

$$C_f = 147.62 \; \phi_{p_1} \; \frac{1+z}{d^2_{L,\rm Gpc}}$$

$$C_i = 1.21 \times 10^9 \; (1+z)^{-1/2} \; t_d^{-1.5}$$

The symbols used are explained in section 2.8.3.